Michigan State University

National Superconducting Cyclotron Laboratory

MOMENTUM DISTRIBUTIONS IN RADIOACTIVE BEAM INTERACTIONS

C.A. BERTULANI and K.W. McVOY

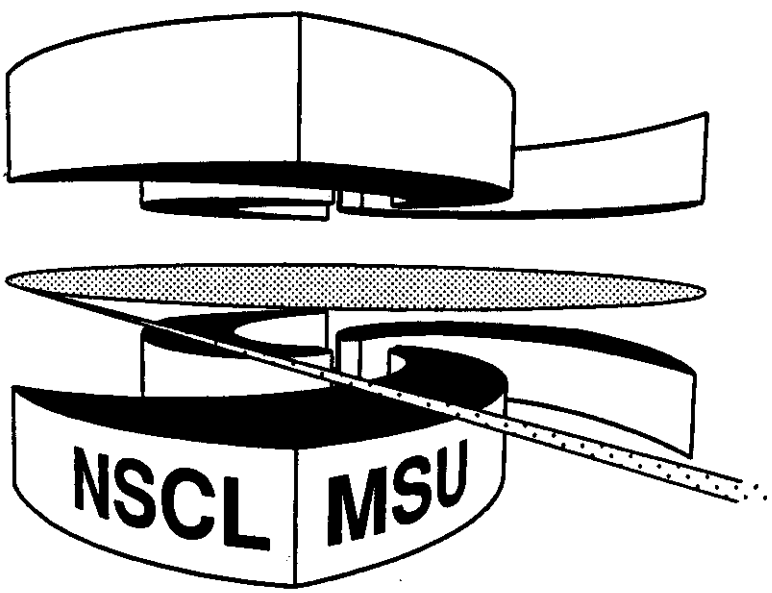

MSUCL-834

MAY 1992

MSUCL-834
May, 1992

Momentum Distributions in Radioactive Beam Interactions

C.A. Bertulani*
National Superconducting Cyclotron Laboratory
Michigan State University, E. Lansing, MI 48824-1312, USA

K.W. McVoy
Physics Department, University of Wisconsin
Madison, Wisconsin 53706, USA

May 14, 1992

Abstract

We investigate the longitudinal and transverse momentum distributions of charged fragments originating from reactions with radioactive, neutron-rich, beams. It is shown that the width of the narrow peak of the longitudinal momentum distribution is insensitive to the details of the collision and the size of the target nucleus. This peak is primarily sensitive to the separation energy, or halo size, of the loosely-bound projectile neutrons, and should provide a reliable measure of this quantity.

In contrast, the width of the peripheral region from which transversely moving particles originate is significantly narrowed via absorption of the outgoing neutrons. This diffractively broadens the width of their transverse momentum distribution, in a manner which depends on details of the collision, and so makes the transverse distribution less reliable than the longitudinal one for measuring the size of the original neutron halo.

Fragmentation reactions with secondary beams of radioactive nuclei have shown that the total reaction cross sections and the transverse momentum distribution of the fragments are sensitive to the separation energy of the last neutrons and to the size of the density profile in these nuclei [1]. These two quantities are linked since the "size" of the nucleus is roughly proportional to the inverse of the square root of the separation energy. Using the Goldhaber model for soft fragmentation, the authors of ref. [1] were able to relate the widths of the narrow peaks in the momentum distributions with the separation energies and sizes of the radioactive nuclei. However, this approach is not free of bias. The interaction of the fragments with the target broadens the narrow peak and makes the extraction of quantitative information about these quantities strongly model-dependent and potentially inaccurate.

We show here that a better measure of the interaction size of the radioactive projectile is obtained by the longitudinal momentum distribution of its fragments. It is also shown that the Coulomb and nuclear fragmentation amplitudes have longitudinal momentum distributions with very nearly equal widths. This fact has indeed been verified in a recent experiment at the NSCL/MSU [2]. On the other hand, the transverse momentum distributions are substantially broadened by the size and diffuseness of the region of overlap with the target and contain Coulomb and the nuclear contributions with different widths. The interpretation of the "wide" (core-neutron) component of the transverse momentum distributions is therefore less straightforward than is that of the longitudinal ones.

In what follows we shall use a simple cluster description of the radioactive nuclei. The conclusions drawn are however of general validity. The cluster model only serves as a guide to obtain an analytical insight into the results. The systems studied experimentally involve reactions of the form

$$a \; + \; A \; \rightarrow \; b \; + \; x \; + \; A^* \equiv b + X \; . \tag{1}$$

According to ref. [3], a spectator model of $a \equiv (b + x)$ gives the singles spectra of the particle b as

$$\frac{d\sigma}{d\Omega_b dE_b} = \rho(E_b) \, \frac{2E_x}{\hbar v_a \, k_x} \int d^2 b_x \, |\tilde{\phi}_a(\mathbf{q}, \, \mathbf{b}_x)|^2 \left[1 - |S_{xA}(b_x)|^2\right] , \tag{2}$$

where

$$|\tilde{\phi}_a(\mathbf{q}, \, \mathbf{b}_x)|^2 = | \int d^3 r_b \; e^{i\mathbf{q}_b \cdot \mathbf{r}_b} \; S_{bA}(b_b) \; \phi_a(\mathbf{r_b} - \mathbf{r_x})|^2 \, , \tag{3}$$

The quantity $S_{iA}(b_i)$ is the S-matrix for the scattering of cluster i ($i = b, x$) from the target A. We obtain it from a complex optical potential by means of the eikonal approximation. For the optical potential we use the "t$\rho\rho$" formalism (see, e.g., ref. [4]), which is obtained by folding the nuclear densities of the participant nuclei weighted by the nucleon-nucleon scattering cross section, with medium correction effects. We shall here concentrate on reactions involving ^{11}Li, ^{11}Be, and ^{6}He, and compare our results with the measurements of the momentum distributions of the ^{9}Li, ^{10}Be, and ^{4}He fragments, respectively. Thus in the cases of ^{11}Li and ^{6}He, we are assuming the two removed neutrons to behave in the projectile as a single cluster, which the collision removes as a unit. The Hartree-Fock densities for these nuclei were taken from ref. [5], except for the ^{6}He, which was taken from ref. [6]. The density distributions of the knocked-out neutrons were taken as the difference between the neutron distributions of the original nuclei and of the observed fragments.

In eq. 3, ϕ_a represents the cluster wavefunction for the incoming $a = (b + x)$ projectile. If one assumes that the fragment b does not interact with the target, i.e, $S_{bA}(b) \equiv 1$, one finds

$$\frac{d\sigma}{d\Omega_b dE_b} = \rho(E_b)\, \sigma_{xA}^{R}\, |\phi_a(\mathbf{q}_b)|^2\,, \tag{4}$$

where σ_{xA}^{R} is the total reaction cross section of fragment x with the target A, and $\phi_a(\mathbf{q}_b)$ is the Fourier transform of $\phi_a(\mathbf{r}_b - \mathbf{r}_x)$ with respect to $\mathbf{q}_b$. The above result is known as the Serber model limit [7]. It tells us that in this approximation the break-up mechanism measures the momentum-space internal wavefunction of the projectile, so that the singles spectrum of fragment b provides important information about the internal structure of the projectile. This is especially useful for the study of extremely short-lived nuclei in secondary beam reactions.

Unfortunately, the Serber model is only a rough approximation for most cases and the elastic scattering (including absorption) of the fragment b on the target has to be included, leading to an unavoidable broadening of the momentum distributions [8]. The physical origin of this broadening is simple diffraction (i.e., the uncertainty principle), as an examination of Eq. 3 makes clear. For instance, if $S_{bA} \equiv 1$, the Fourier transform given by this equation would be exactly the Fraunhofer diffraction pattern (as a function of $\mathbf{q}_b$) of the "source distribution" $\phi_a(\mathbf{r}_b - \mathbf{r}_x)$. Including the factor $S_{bA}(b_b)$, with

$|S_{bA}(b_b)| \leq 1$, effectively decreases the transverse width of the source by eliminating the part that overlaps with the target A, and this will of course broaden the transverse diffraction pattern.

This broadening makes it harder to extract the internal momentum structure of the projectile. However, since for high energy collisions the S-matrix S_{bA} does not depend on the longitudinal coordinate, the longitudinal momentum distribution is expected to be much less altered by the S_{bA} absorption. In particular, a gaussian shape is quite appropriate for the light projectiles considered here, and in this case the longitudinal and transverse parts of the integral of eq. 3 factorize completely. That is, if we take for the projectile cluster wave function the approximation

$$\phi_a \propto \exp\Big\{-(\mathbf{b}_b - \mathbf{b}_x)^2 \Delta^2\Big\}\,, \tag{5}$$

one finds

$$\begin{aligned}
\frac{d\sigma}{dq_{//}^{(b)}} &= (2\pi)^2 \frac{E_x}{\hbar v_a\, k_x} \frac{C_\Delta^2}{\Delta^2} \exp\Big\{-\frac{[q_{//}^{(b)}]^2}{2\Delta^2}\Big\} \\
&\times \int d^2 b_x\; b_x\; \exp\Big\{-2\,\Delta^2\, b_x^2\Big\}\; \Big[1 - |S_{xA}(b_x)|^2\Big] \\
&\times \int db_b\; b_b\; \exp\Big\{-2\Delta^2\, b_b^2\Big\}\; I_0\Big(4 b_x b_b \Delta^2\Big)\; |S_{bA}(b_b)|^2\,,
\end{aligned} \tag{6}$$

where the C_Δ is a normalization constant and I_0 a Bessel function. That is, the dependence on $q_{//}^{(b)}$ is given by a Gaussian function multiplied by a geometrical factor. Therefore, the longitudinal momentum distribution measures the internal momentum function of the projectile and is insensitive to the details of the nuclear interaction. This fact was pointed out by Friedman in the general context of nuclear fragmentation reactions [9].

Due to their low separation energies, the projectiles near the β-instability line are also easily Coulomb excited/fragmented. It is well known that the electromagnetic excitation cross sections induced in nuclear collisions are directly related to the cross sections induced by real photons [10]. The proportionality factor is the so-called number of virtual photons, which is a slowly varying function of the photon energy. Therefore, the momentum distribution of the fragments will be determined by a matrix element of the form (in

the dipole approximation)

$$\mathcal{M}_{if} = \int r\, Y_{1m}(\hat{\mathbf{r}})\, \phi_f^*(\mathbf{r})\, \phi_i(\mathbf{r}) d^3r\ . \tag{7}$$

We again assume that the initial wavefunction ϕ_i has a gaussian form, and use plane waves for the final state. This neglects the final-state interaction of b with A, an approximation appropriate to the Coulomb fragmentation, which takes place farther from A than does the nuclear fragmentation. With these assumptions, one finds that the momentum distribution of the fragments due to the Coulomb interaction has a gaussian shape in all three components of $\mathbf{q}_b$.

$$\frac{d^2\sigma}{dq_b^2} = Const.\ q_b\ \exp\Big\{-\frac{q_b^2}{2\Delta^2}\Big\}. \tag{8}$$

Integrating over $k_T^{(b)}$ one gets in good approximation another gaussian distribution for the longitudinal momentum distribution, this time from the electromagnetic fragmentation process.

Recently, the longitudinal momentum distribution of ^9Li from the fragmentation of ^{11}Li projectiles with 70 $MeV/nucleon$ has been measured at the NSCL/MSU using several targets [2]. The data were taken using light and heavy targets, thus probing the relative strengths of the nuclear and the Coulomb interaction on the break-up. As shown in fig. 1, this width can be explained by using eq. 5 and a calculation for the electromagnetic break-up of the projectile [10] with the value $\Delta = 20\ MeV/c$, for all targets. A recent detailed calculation by Esbensen and Bertsch for the electromagnetic dissociation of $11Li$ on tantalum [12], accounting for initial- and final- state correlations between the valence neutrons in ^{11}Li, has also obtained this value for the momentum width. This momentum width can be approximately related to the separation energy of the ^{11}Li by $E_B \simeq \Delta^2/\mu_{bx} = 0.26\ MeV$, which agrees well with the experimental value in direct measurements. Although approximate, this relation shows that in fact the separation energy can be obtained from the measurements of the widths of the longitudinal momentum distributions.

Using the gaussian shape for ϕ_a and integrating eq. 2 over $q_{//}^{(b)}$, one obtains for the transverse momentum distribution

$$\frac{d^2\sigma}{dq^2_{T(b)}} = \sqrt{2\pi}\,\frac{E_x}{\hbar v_a k_x}\,\frac{C^2_\Delta}{\Delta} \times \int d^2b_x\; b_x\; \exp\left\{-2\,\Delta^2\,b_x^2\right\}\;\left[1-|S_{xA}(b_x)|^2\right] \times \sum_{m=-\infty}^{m=\infty} \Big|\int db_b\; b_b\; \exp\left\{-\Delta^2\,b_b^2\right\}\,J_m(q_T^{(b)}b)\,I_m\left(2b_x b_b\Delta^2\right)\,S_{bA}(b_b)\Big|^2\,, \tag{9}$$

where J_m and I_m are Bessel functions. In contrast to eq. 5, the above relation shows that the transverse momentum distribution depends on the target size parameters.

Figure 2 shows the transverse momentum distributions of ^9Li, ^{10}Be and ^4He from the break-up of ^{11}Li, ^{11}Be and ^6He projectiles, respectively, incident on carbon at 800 *MeV/nucleon*. For this target only the nuclear contribution to the break-up needs to be considered. The data are from ref. [1]. The dotted curves are the result of the Serber model calculation following eq. 3. The momentum parameters Δ were determined by the separation energies of the fragments with the approximate formula $\Delta = \sqrt{\mu_{bx}\,E_B}$ which give the values 0.25 MeV, 0.5 MeV and 0.97 MeV for ^{11}Li, ^{11}Be and ^6He, respectively. The dashed curves were obtained using the more correct approach of eq. 2.

In the case of ^{11}Li the result of the Serber model agrees with the one obtained for the longitudinal momentum distribution data of NSCL/MSU, since the momentum distribution given by this model is isotropic. The interaction of the fragments with the target broadens the peak, and this is displayed by the dashed curves in this figure. However, it is also seen that the wings of the momentum distributions cannot be reproduced by using a single gaussian parameterization for the ground state wavefunction. This is due to the simple cluster model picture that we have undertaken. More realistic models are able to describe these wings (wide component) [11], but our analysis is consistent with the idea that the narrow peak measures the separation energy of the halo fragments.

An attempt to explain the wings of the momentum distributions displayed in figure 2 (solid lines), can be made by assuming that also neutrons

from the core of the projectile could be removed with appreciable probability [1]. One can assume that the cross sections for the removal of the loosely-bound valence neutrons and the more tightly-bound from the core add incoherently. The results are shown by the solid lines in figure 2. In this calculation we added two results of the eq. (8): the ones which yield the dashed lines in fig. 2, with other ones with the internal momentum widths $\Delta_2 = 55\ MeV/c$, $92\ MeV/c$ and $79\ MeV/c$, for ^{11}Li, ^{11}Be and ^{6}He, respectively. The Hartree-Fock densities for the core nucleons were taken from ref. [BBS89][Su91]. These momentum widths are much wider than the one cited before, and are related to the separation energies of the core neutrons. The contributions of the two gaussian simulation for the internal wavefunctions were chosen so as to reproduce as well as possible the experimental data. The excellent agreement with the experimental data (solid lines in fig. 2) should therefore be approached with some caution, since any two gaussian fit can reproduce the transverse momentum data [1]. Nonetheless, the ratio between the two contributions gives roughly the spectroscopic factors for the removal of neutrons from the core and from the halo, respectively. This ratio, $\sigma_{wide}/\sigma_{narrow}$, is however large, being about 0.4 for the fragmentation of ^{11}Li. It is hard to believe that so many events could arise from by the removal of tightly bound neutrons. We are more inclined to think that the observed wings are the results of three-body effects, as claimed by Zhukov *et al.* [11].

Another interesting feature shown in figure 2 is a small shift of the peaks with respect to the central position ($q_T = 0$). This shift arises from the phase of the S_b-matrices originating in the real part of the potential, but is small and has been neglected in our calculations.

The above analysis shows that the longitudinal momentum distribution which results from the fragmentation of weakly-bound light projectiles is insensitive to the interaction, and provides a reliable probe of the internal momentum wavefunction of the projectile. On the other hand, the transverse momentum distribution depends on the reaction mechanism, and the extraction of definite information about the halo size is not free of bias. One interesting problem to be studied is the extension of the experimental measurements to look for the possible existence of wings in the longitudinal momentum distributions, which do not appear in the data of ref. [2]. The existence of such wings would provide a more definitive measure of the contribution of more tightly bound nucleons, from the core of the projectiles, which have been assumed to explain the wings of the transverse momentum

distribution [1].

* On leave of absence from Instituto de Física, Universidade Federal do Rio de Janeiro, 21945 Rio de Janeiro, Brazil

Acknowledgements

We are indebted to N. Orr and B. Sherill for providing us with their results prior to publication and to G. Bertsch for useful discussions.

Figure Captions

1. Longitudinal momentum distributions of ^{9}Li fragments from the break-up of ^{11}Li incident on *(a)* Be, *(b)* Ni, and *(c)* Ta targets, at 70 MeV/nucleon. The data are from ref. [2], and the curves are from Eqs. 2 and 6, normalized to the data.

2. Transverse momentum distributions of *(a)* ^{9}Li fragments from the break-up of ^{11}Li *(b)* ^{10}Be fragments from the break-up of ^{11}Be *(c)* ^{4}He fragments from the break-up of ^{6}He projectiles projectiles incident on carbon at 800 $MeV/nucleon$. The data are from ref. [1]. The dotted and dashed curves describe halo neutrons only, the dotted curve neglecting final-state neutron interactions with the target, and the dashed curve including them via eqs. 6 and 9. The solid curves are 2-gaussian fits to the data, using widths determined by the binding of the core and halo neutrons of the projectile.

References

[1] T. Kobayashi *et al.*, Phys. Rev. Lett. **60** (1988) 2599;
T. Kobayashi, I. Tanihata, Proc. Int. Symposium on Structure and Reactions of Unstable Nuclei, June 17-19, 1991, Niigata, Japan, World Scientific, ed. by T. Suzuki.

[2] N. Orr *et al.*, MSU-preprint, 1992, to be published

[3] M. S. Hussein and K. W. McVoy, Nucl. Phys. **A445** (1985) 124

[4] M.S. Hussein, R.A. Rego and C.A. Bertulani, Phys. Reports **201** (1991) 279

[5] G. Bertsch, B.A. Brown and H. Sagawa, Phys. Rev. **C39** (1989) 1154

[6] Y. Suzuki, Nucl. Phys. **A528** (1991) 395

[7] R. Serber, Phys. Rev. **72** (1947) 1008

[8] H. Utsunomiya, Phys. Rev. **C41** (1990) 1309

[9] W.A. Friedman, Phys. Rev. **C27** (1983) 569

[10] C.A. Bertulani and G. Baur, Phys. Reports **163** (1988) 299

[11] M.V. Zhukov *et al.*, Nucl. Phys. **A529** (1991) 53; Nucl. Phys. **A539** (1992) 177

[12] H. Esbensen and G. F. Bertsch, Nucl. Phys. **A**, in press

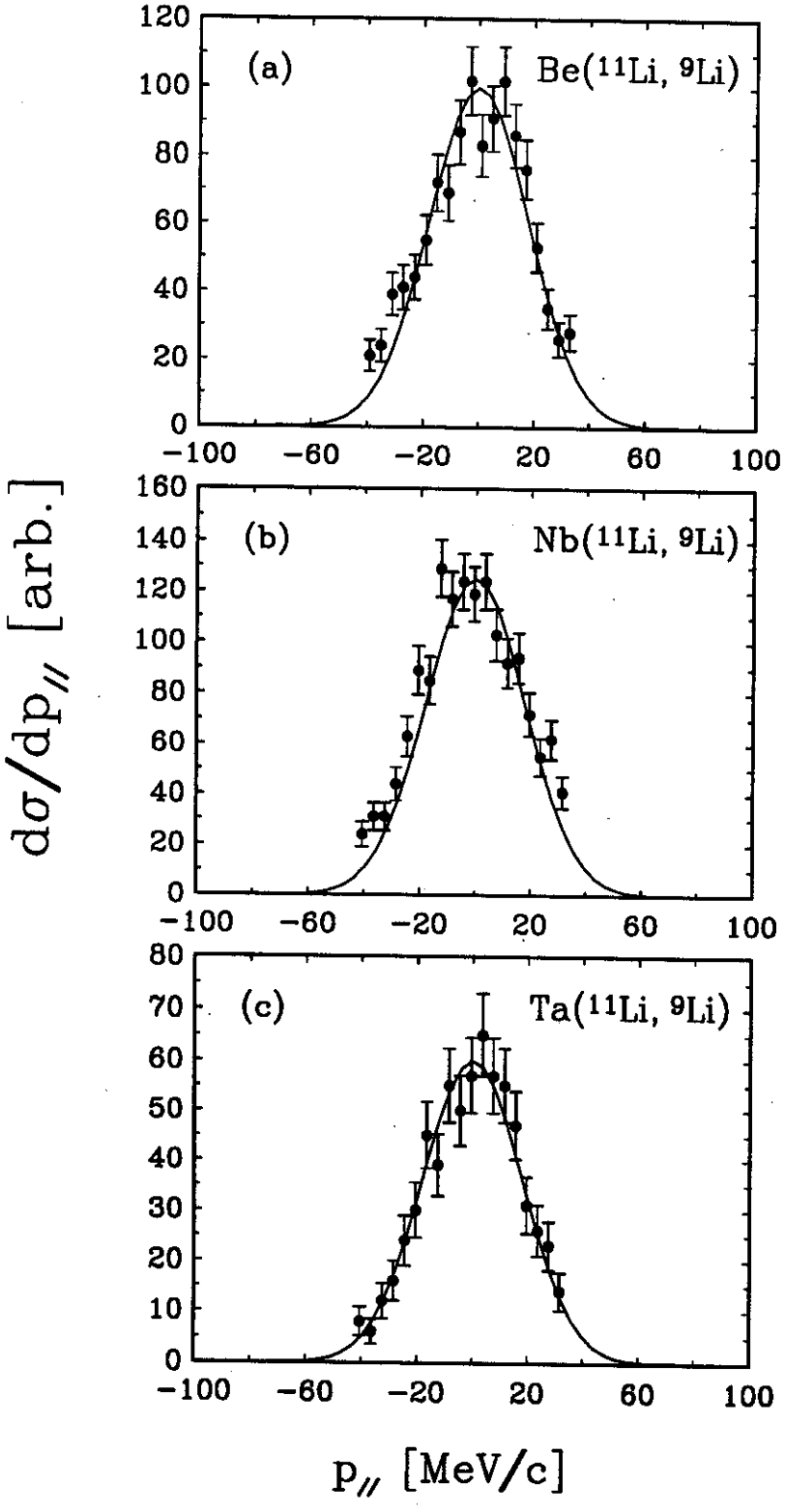

Figure 1

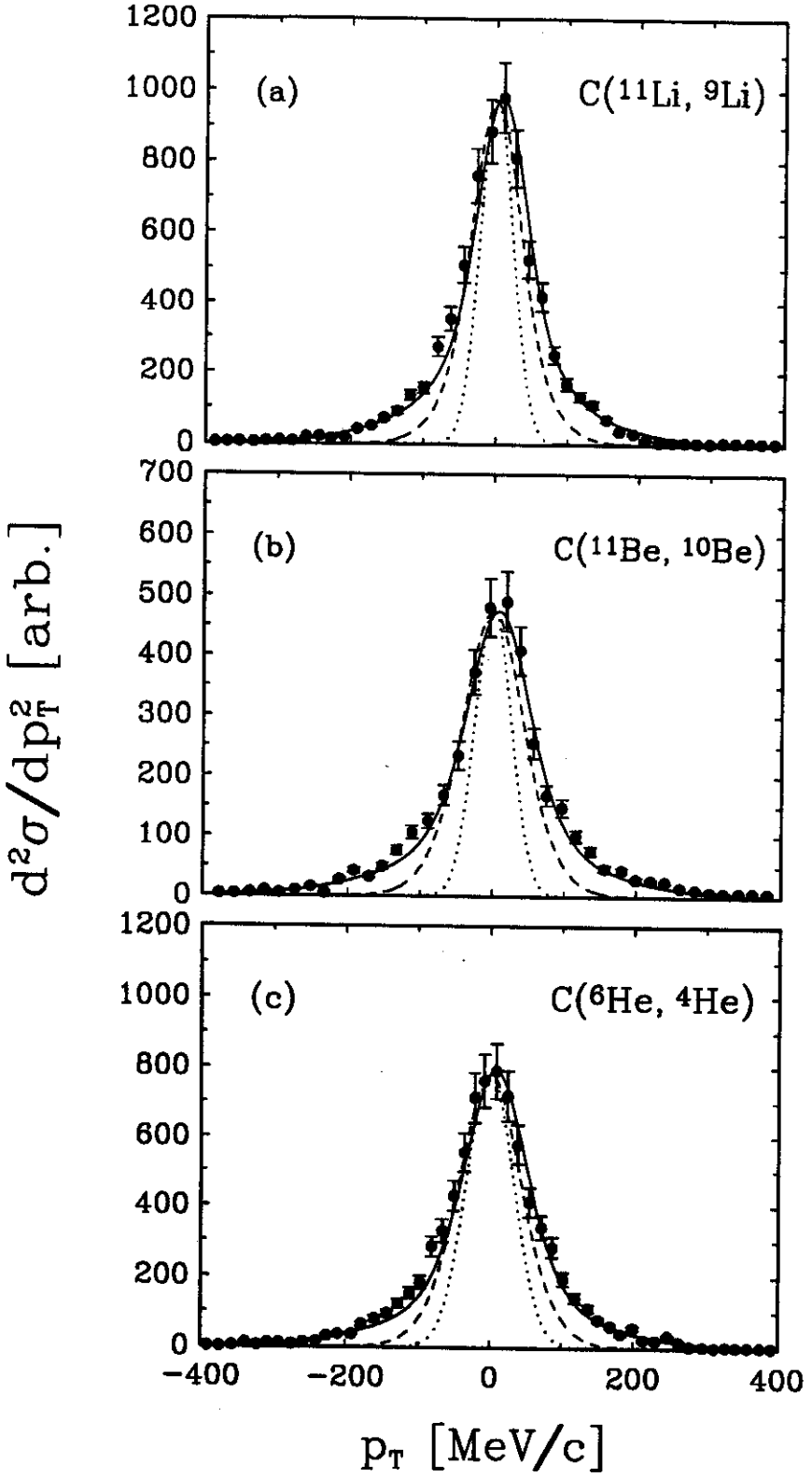
(a)
C(11Li, 9Li)
(b)
C(11Be, 10Be)
(c)
C(6He, 4He)
d2σ/dpT2 [arb.]
pT [MeV/c]
1200
1000
800
600
400
200
0
700
500
300
100
−400
−200
200
400

Figure 2